Cryogenic stopping cell for photofission fragments at the ELI-NP facility

P. Constantin, D. L. Balabanski, and P. V. Cuong

Citation: AIP Conference Proceedings **1681**, 030002 (2015); doi: 10.1063/1.4932246
View online: http://dx.doi.org/10.1063/1.4932246
View Table of Contents: http://scitation.aip.org/content/aip/proceeding/aipcp/1681?ver=pdfcov
Published by the AIP Publishing

Cryogenic Stopping Cell for Photofission Fragments at the ELI-NP Facility

P. Constantin[1,a)], D. L. Balabanski[1] and P. V. Cuong[2]

[1]*ELI-NP, IFIN-HH, Str. Reactorului 30, 077125 Bucharest Magurele, Romania*
[2]*Centre of Nuclear Physics, Institute of Physics, No. 10, Daotan, Thu le, Badinh, Hanoi, Vietnam*

[a)]Corresponding author: paul.constantin@eli-np.ro

Abstract. *The brilliant gamma beam at the future Extreme Light Infrastructure - Nuclear Physics (ELI-NP) facility will be used to generate a beam of exotic neutron-rich isotopes via photofission of actinide targets. We present simulations with the Geant4 toolkit of the photofission process for the design and optimization of the expected performance parameters of the Cryogenic Stopping Cell (CSC). The CSC will be used to extract the photofission fragments into the secondary beam of about 10^6 ions/s. We propose an experimental program to study refractory neutron-rich isotopes.*

INTRODUCTION

The ELI-NP facility will make available to the scientific community two high power lasers (10 PW, 10^{23} W/cm^2) and a very brilliant gamma beam that can be used separately or jointly in a variety of experiments [1] in fields like nuclear physics, quantum electrodynamics, material science and medical research. One example of nuclear physics experiments planned at ELI-NP is the study of photofission of actinide targets exposed to the gamma beam.

The gamma beam is generated by laser Compton backscattering (CBS): the photon beam from a Yb:Yag laser (E_0=2.4 eV) is backward scattered on a high intensity electron beam accelerated up to 720 MeV by a warm linac, receiving an energy boost to $E_\gamma \approx 4\gamma_e^2 E_0$ =0.2-19.5 MeV, where γ_e is the electron relativistic factor. This gamma beam will have a spectral density of up to $4{\cdot}10^4$/(s·eV), a bandwidth of 0.3-0.5% and a linear polarization above 99% [2] . Due to the strong angle-energy anti-correlation of the CBS process, the lower limit of the energy spectrum is set by beam collimation. The upper limit of the energy spectrum can be set by tunning the energy of the electron beam.

Left panel of Figure 1 shows with blue squares the energy spectrum of the gamma beam collimated by a lead block with an angular opening of 0.7 mrad, producing the lower edge at 10 MeV, and with black circles the spectrum of background photons generated in the collimator (less than 0.3%). The right panel shows the beam spot obtained at 775 cm away from the CBS interaction point, where the target will be placed. In all the simulations of "day-one" experiments, we have used a conservative total gamma rate of $5{\cdot}10^{10}\gamma$/s.

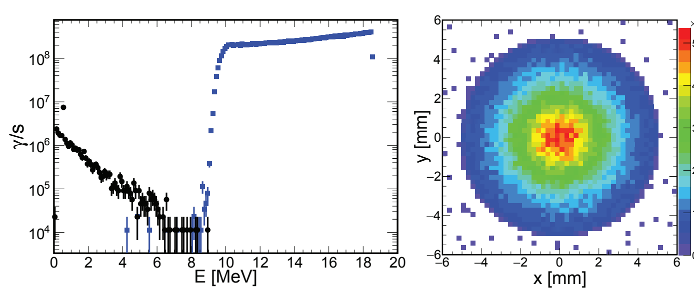

FIGURE 1. Left: spectrum of the γ beam (blue squares) collimated below 0.7 mrad and background photon spectrum (black circles) generated in collimator. Right: the collimated gamma beam spot at 775 cm, with a standard deviation $\sigma(1D)$=2.1 mm.

Nuclear Structure and Dynamics '15
AIP Conf. Proc. 1681, 030002-1–030002-4; doi: 10.1063/1.4932246

The ELI-NP Photofission Experimental Programs

For photofission experiments, three programs are proposed at ELI-NP [1]:

I. Studies of transmission resonances of isomeric fission: the energy resolution of 15-18 keV below the fission barrier permits the excitation of individual transmission resonances in the 2^{nd} and 3^{rd} minima of super- and hyper-deformed nuclei fission barrier. The sub-millimeter beam spot and very low backgrounds allow the measurement of high-resolution fragment angular distributions, hence of resonance spin and parity values. Two detector arrays, one of Thick Gas Electron Multiplier (THGEM) detectors and one of Bragg Ionization Chambers (BIC) with Double Sided Silicon Strip detectors (DSSSD), are developed at MTA Atomki (Hungary) for these measurements.

II. Investigation of the angular anizotropy of fission fragments and of short-lived isomers nuclear moments: the complete polarization and low backgrounds of the γ beam offer a niche for such studies at ELI-NP. This in-beam γ spectroscopy program will use the ELIADE array which is developed at ELI-NP and consists of HPGe Clover detectors, coupled to fast-timing $LaBr_3$ crystals, and a superconducting magnet.

III. Production of exotic neutron-rich RIBs (radioactive ion beams): the entire Giant Dipole Resonance (GDR) of actinide targets can be excited by the γ beam (see left panel of Figure 1) and can be used to produce exotic RIBs via photofission. The production and study of refractory isotopes in the light region Zr-Mo-Rh and in the rare-earth region around Ce is the main purpose of this program. An IGISOL beam line with a gas cell containing the targets will be developed in collaboration with GSI and the University of Giessen (Germany).

An important common task of these three research topics is the optimization of the photofission rate and of the ion extraction efficiency via Geant4 simulations. While the work reported here presents the current status of this study, a forthcoming paper will present in detail the results of the finished analysis.

The IGISOL Beam Line

The following devices developed for the Fragment Separator (FRS) Ion Catcher facility at GSI [3] will also be employed at the ELI-NP IGISOL beam line: the Cryogenic Stopping Cell (CSC), the Radio-Frequency Quadrupole (RFQ) and the Multiple-Reflection Time-of-Flight (MR-ToF) mass spectrometer.

In its current design, the CSC stops the ion beam along its axis and drifts the ions out on the same direction using DC and RF fields. Several innovative technologies are employed in its design [3]: (i) large DC fields (up to 30 V/cm), created by ring electrodes, for fast ion extraction; (ii) RF carpets: resonant radio frequency fields (6 MHz) that prevent ion adhesion to cell walls and push the ions to the exit nozzle; (iii) cryogenic operation (60-90 K) for increased ion stopping and gas purity. They allowed fast (25ms) and efficient (15%) extraction of the fission fragments.

The RFQ extracts, cools, separates by mass and bunches the ion beam. The MR-ToF does mass separation with $m/\Delta m \approx 10^5$ in 5 ms either to perform direct mass measurements or to provide isobarically clean RIBs.

A new design of the CSC is being developed at GSI [4]. It has lateral extraction, hence shorter ion path, and two chambers at large pressure difference. These and other developments are expected to lead to improvements in ion extraction: efficiency≈50%, time≈5ms, rate 10^7 ions/s.

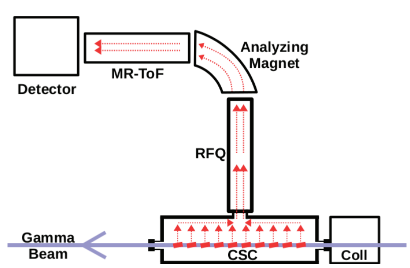

FIGURE 2. Conceptual drawing of the layout of the IGISOL beam line: target foils are shown with full red lines and ion trajectories are shown with dashed red arrows.

Figure 2 shows the conceptual design of the IGISOL beam line for RIBs at ELI-NP with its main components. It considers the possibility that, in the first implementation, mass separation could be done by RFQ and a simple analyzing magnet - the MR-ToF being added to the system later. The main difference between the facilities at GSI and ELI-NP is the mechanism of production of exotic nuclei: an ion beam is injected in the CSC at GSI, while the production of fission products in actinide targets happens in the CSC at ELI-NP.

For our target geometry, shown with red full lines in Figure 2, we have chosen many thin foils of ^{238}U, tilted with respect to the γ beam axis (blue line) at a shallow angle. The main reasons are the following: the foil thickness cannot be larger than about 10 μm such that the fission fragments can leave the target [5]; average fragment release direction cannot point towards neighboring foils; effective path length of the γ rays through the target should be maximized.

Fragment trajectories in the CSC, depicted with red dashed arrows, have three segments: (1) the stopping segment is orthogonal to the drawing plane (in both in and out directions); (2) the DC drift segment is upwards, towards the exit nozzle; (3) the RF carpet segment is along the wall with the nozzle. Once they reach the region around the exit nozzle, ions are taken out by the gas flow in a supersonic gas jet through the RFQ. The target geometry parameters are: the number of foils N, the foil thickness t, the tilting angle α, the transversal size a, equal on both directions (chosen to overlap the beam spot in the right panel of Figure 1) and the inter-foil distance d. The optimization of these parameters has been done within the Geant4 framework to achieve maximum RIB rates.

Simulations of the CSC

Two complementary implementations of the photofission process have been added to the Geant4 framework in order to simulate the production of RIBs in the ELI-NP IGISOL beam line. They are based on measurements of actinide (γ,f) cross-sections from [6] and the (Z,N) distribution of fission fragments in ultra-peripheral ^{238}U(γ^*,f)^{208}Pb collisions, with the virtual γ energy below 25 MeV, from [7]. The neutron multiplicity and the mean and standard deviation of the fragments Total Kinetic Energy (TKE) were taken from [8].

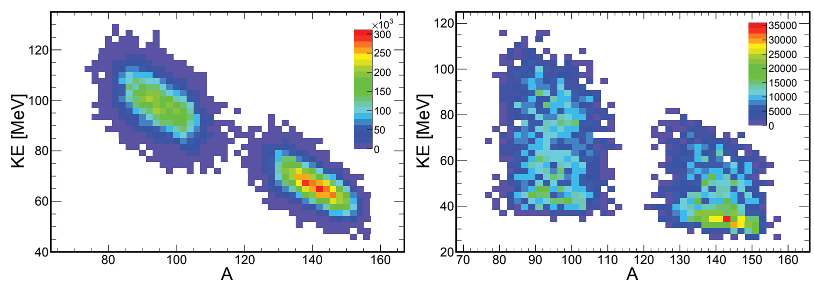

FIGURE 3. Left: kinetic energy KE versus atomic mass A of photofission fragments produced in the target. Right: kinetic energy KE versus atomic mass A of photofission fragments released from a target with 7 μm thickness. Both correspond to a total rate of $1.7 \cdot 10^7$ fissions/s produced by exposing 800 mg of ^{238}U to $5 \cdot 10^{10} \gamma$/s.

The left panel of Figure 3 shows the kinetic energy of the photofission fragments produced in a target with 800 mg of ^{238}U by a beam of $5 \cdot 10^{10} \gamma$/s versus their atomic mass. This target is made of many foils with the thickness of 7 μm. The right panel shows the same distribution, but for the fragments that manage to escape from the target foils.

We get a rate of $1.7 \cdot 10^7$ fissions/s produced in the target and a rate of $5.5 \cdot 10^6$ fragments/s released from the target: about 16% of the fragments are released into the CSC. They lose about a third of their kinetic energy on their way out: the mean value decreases from 82.5 MeV to 57.5 MeV, as can be seen in Figure 3. Their atomic mass A and atomic number Z distributions do not change significantly.

The optimal values of the target parameters defined in the previous section are chosen to maximize the fragment release rate and are found to be the following: N = 19, t = 7 μm, $\alpha = 7^o$, a = 6 mm, d = 2 mm. They also fulfill the two constraints that we have in the first phase of the IGISOL project: a maximum ^{238}U mass of 800 mg and a maximum active length of the CSC of 110 cm, corresponding to a total maximum length of 150 cm that includes the vacuum enclosure. These values for the tilting angle α and the foil transversal size a imply a target foil length of 4.92 cm.

After being released from the target, ions are slowed in the He gas of the CSC down to a kinetic energy of about 1 keV, after which the DC field takes over and starts to push them along the orthogonal direction, as described above.

An important parameter for the design of the CSC is the stopping length δ of the ions in the gas, shown in the left panel of Figure 4. We have used the optimal parameters of the He gas: a temperature of 70 K and a pressure of 300 mbar, hence a density ρ=0.206 mg/cm^3. More than 95% of the ions stop in 12 cm, suggesting that the total width of the CSC should be about 25 cm.

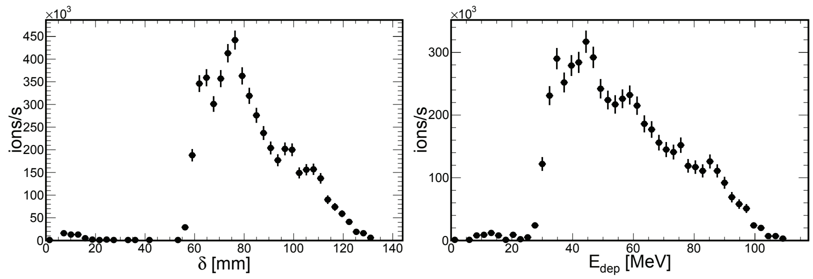

FIGURE 4. Left: total path length δ of the ions released from the target in the gas cell. Right: energy deposited E_{dep} by the ions released from the target in the gas cell.

The right panel of Figure 4 shows the distribution of energy deposited in the He gas via ionization. From its mean value of 57.5 MeV, we can calculate the mean density rate of energy deposition via ionization:

$$\langle j_E \rangle = \frac{\langle E_{dep} \rangle \cdot n_{rel}}{L \cdot w^2} = \frac{57.5MeV \cdot 5.5 \cdot 10^6 s^{-1}}{110cm \cdot (25cm)^2} = 4.6 \frac{GeV}{cm^3 \cdot s} \tag{1}$$

where $L \cdot w^2$ is the stopping volume. If we further divide by the mean energy deposition of 41 eV, required to create an electron-ion pair by ionizing a He gas, we get the mean density rate of pair creation of $\langle j_{e-ion} \rangle \approx 10^8$ pairs/(cm^3·s). A comparison with estimates done for the CSC at GSI suggests that this mean value is below the range where significant space charge effects start to deteriorate the extraction time and efficiency of the CSC. However, further studies of the mechanism of space charge creation will be done.

Conclusions

The conservative rates, using a $5 \cdot 10^{10} \gamma$/s beam rate and optimal target and gas cell configurations within the mass and length constraints of project's first phase, are $1.7 \cdot 10^7$ photofissions/s and $5.5 \cdot 10^6$ extracted ions/s. The optimal rates, using a 10^{12} γ/s beam rate and no target mass or cell length limitations, have 1-2 orders of magnitude more.

They imply, for example, that neutron-rich isotopes of Molybdenum up to N=71 (conservative) and 73 (optimal) and of Cerium up to N=97 (conservative) and 99 (optimal) can be measured at a rate of one isotope per second. The light refractory isotopes around Mo and heavy-earth refractory isotopes around Ce will be the central focus of our IGISOL beam line project, as they are difficult to extract at other facilities.

ACKNOWLEDGMENTS

The Extreme Light Infrastructure Nuclear Physics (ELI-NP) - Phase I project is co-funded by the European Union through the European Regional Development Fund. Phan Viet Cuong acknowledges the support of the Vietnam National Foundation for Science and Technology Development (NAFOSTED) under grant number 103.04-2014.29.

REFERENCES

[1] D. B. et al., J. Phys.: Conference Series **590**, p. 012005 (2015).
[2] O. A. et al., arXiv:1407.3669 (2014).
[3] W. P. et al., Nucl. Instr. Meth. **B** **317**, p. 457 (2013).
[4] T. D. et al., GSI Scientific Report (2014).
[5] A. A.-A. et al., arXiv:1409.0714 (2014).
[6] J. C. et al., Phys. Rev. **C** **21**, p. 1215 (1980).
[7] C. D. et al., Eur. Phys. J. **A** **1**, p. 407 (1998).
[8] S. P. et al., Nucl. Phys. **A** **572**, p. 237 (1994).